

Electro dynamic model of eddy currents in EU DEMO TF coil casing during major plasma disruption

*Original*

Electro dynamic model of eddy currents in EU DEMO TF coil casing during major plasma disruption / De Bastiani, M., Bonifetto, R., Messina, G., Morici, L., Zanino, R., Zappatore, A.. - In: FUSION ENGINEERING AND DESIGN. - ISSN 0920-3796. - 196:(2023), p. 113987. [10.1016/j.fusengdes.2023.113987]

*Availability:*

This version is available at: 11583/2982530 since: 2024-01-24T07:59:54Z

*Publisher:*

Elsevier

*Published*

DOI:10.1016/j.fusengdes.2023.113987

*Terms of use:*

This article is made available under terms and conditions as specified in the corresponding bibliographic description in the repository

*Publisher copyright*

(Article begins on next page)



# Electro dynamic model of eddy currents in EU DEMO TF coil casing during major plasma disruption

Marco De Bastiani <sup>a</sup>, Roberto Bonifetto <sup>a,\*</sup>, Giuseppe Messina <sup>b</sup>, Luigi Morici <sup>b</sup>, Roberto Zanino <sup>a</sup>, Andrea Zappatore <sup>a</sup>

<sup>a</sup> NEMO group, Energy Department, Politecnico di Torino, Corso Duca degli Abruzzi, 24, Torino, 10129, Italy

<sup>b</sup> ENEA, Via Enrico Fermi, 45, Frascati, 00044, Italy

## ARTICLE INFO

### Keywords:

Superconducting magnets  
Nuclear fusion reactors  
Numerical modeling  
Electro-magnetics  
Thermal-hydraulics  
Major plasma disruption

## ABSTRACT

The conceptual design of the EU DEMO reactor is currently ongoing within the EUROfusion consortium. Many different fault transients must be considered and carefully analyzed in the design phase; one of the most severe is the major plasma disruption (MPD), which causes several drawbacks on the magnet system. During a disruption, the plasma current decreases extremely fast, causing a fast variation of the magnetic field, which in turn induces an electric field. In presence of conductive materials, e.g., coil casing and vacuum vessel (VV), the electric field induces large eddy currents which deposit power by Joule effect. The conductive regions are tightly coupled on different timescales through the magnetic field induced by the eddy currents: the eddy currents in the VV influence the magnetic field evolution in the TF coil casing, thus affecting the power deposition in the latter. The aim of this work is the evaluation of the power deposited within the TF coil casing during a major plasma disruption due to eddy currents. The power deposition has been evaluated by means of the 3D-FOX, a finite element (FE) tool developed at Politecnico di Torino. The computed power deposition is used as input to the thermal-hydraulic (TH) simulation, performed with the 4C code, with the aim of assessing the erosion of the temperature margin given by MPD.

## 1. Introduction

The EU DEMO nuclear fusion reactor aims at providing electricity to the grid in Europe [1]; its conceptual design is currently ongoing within the EUROfusion consortium. In this design phase many different fault transients must be considered to assess the robustness of the design. Among these accident, one of the most severe is the major plasma disruption (MPD), which may cause drawbacks on the magnet system. During a MPD, the plasma current dumps extremely fast to zero, causing a subsequent fast variation of the magnetic field. According to Faraday's law the time variation of the magnetic field is generating an electrical field which, in turn induces eddy currents within the conductive components (e.g. the vacuum vessel (VV) and the toroidal field (TF) coil casing). The conductive components are coupled through the magnetic field which is induced by the eddy currents: indeed the VV eddy currents strongly influence the field in the TF coil casing, thus affecting the currents there induced. The induced currents are responsible of a consistent power deposition by Joule effect, both in

the VV and in the TF coil casing. The latter can contribute to erode the superconductor (SC) cable temperature margin potentially leading the magnet to quench initiation [2]. The MPD, causing a transient behavior of the magnetic field, induces AC losses as well. By the way AC losses evaluation is out of the scope of this work. Indeed, the aim of this work is computing the evolution of the power deposited in the TF coil casing during a MPD and assessing its contribution to the temperature margin reduction, as a complement to what is proposed in other works in which EM behavior of the SC material is analyzed during different transients [3,4]. Previous works dedicated to the analysis of MPD effect from the eddy current point of view have been performed especially for ITER. Some of them have been dedicated to the evaluation of the mechanical loads due to Lorentz forces [5,6], while other focused on the evaluation of Joule power during plasma transients [7] using the CARIDDI code [8]. Differently from [7], here the EM computation has been performed with the 3D-FOX [9], a three dimensional finite element (FE) tool developed at

\* Corresponding author.

E-mail address: [roberto.bonifetto@polito.it](mailto:roberto.bonifetto@polito.it) (R. Bonifetto).

Politecnico di Torino using FreeFem++ [10]. Similarly to the CARIDDI code it provides accurate distribution of induced eddy current and Joule heat deposition, but with the advantage that can be easily coupled with the 4C code [11], obtaining a direct feedback on the magnet thermal-hydraulics following the Joule power deposition. This allows the investigation of the evolution of the coil temperature margin during the electro-magnetic transient.

## 2. 3D-FOX model

For the simulation of the MPD in EU DEMO reactor three components must be introduced within the model: the plasma, in which the driver current is defined, the VV and the TF coil casing, in which eddy currents are induced. Eddy currents are induced in the conducting materials of the WP as well, but their magnitude is smaller with respect to those induced in the TF coil casing for the concurrent effect of the reduced material cross section (due to interturn and interlayer insulation) and of the reduced magnetic field time derivative detected in the WP. Indeed the magnetic field in the WP is mainly given by its own current rather than the plasma.

### 2.1. Plasma model

The plasma is modeled as two concentric torus in which the two (toroidal and poloidal) components of the current are externally imposed. The inner torus has major radius  $R = 9\text{ m}$  and minor radius  $r = 0.75\text{ m}$  and the toroidal current component is prescribed uniform in its radial-vertical cross section, with no poloidal component. The external one, with an annular cross section, has the same major radius of the inner one and minor internal radius  $r_{in} = 0.9\text{ m}$  and minor external radius  $r_{out} = 1.4\text{ m}$ . The poloidal component of the plasma current is prescribed uniform in the external torus, with no toroidal component. The current orientation are shown in Fig. 1. To simulate the MPD the plasma current is decreased linearly from the nominal value to zero in  $t_{discharge} = 57\text{ ms}$  [12,13]. The nominal plasma current values are set to:  $I_{p,tor} = 18\text{ MA}$  and  $I_{p,pol} = 3.6\text{ MA}$ . Plasma current evolution is shown in Fig. 2.

### 2.2. VV model

The VV is a bulky stainless steel component which has been modeled on the base of the EU DEMO baseline 2017 [14], simplifying it removing the port stubs and ducts. Actually, the latter are far away from the plasma (and from the TF coils), and they are smaller than the VV body, so the magnitude of the eddy currents there can be considered negligible, as it is possible to deduce from previous similar computations [6]. In Fig. 3 the CAD adopted for the VV FE model is shown. The VV material is assumed to be AISI 316LN stainless steel. The relevant material properties to be considered in the computation are the electrical resistivity ( $\rho_{el}$ ) and the magnetic permeability ( $\mu$ ). The magnetic permeability is considered to be equal to the vacuum one  $\mu_{VV} = 4\pi \cdot 10^{-7}\text{ H/m}$ , while the electrical resistivity is considered to be constant and equal to that evaluated at  $330\text{ K}$   $\rho_{el,VV} = 80 \cdot 10^{-8}\ \Omega\text{ m}$ .

### 2.3. TF coil casing model

The TF coil model has been developed based on the winding pack WP1 design proposed by SPC [15]. In the TF coil model both casing and WP are included. The casing material is, as for the VV, AISI 316LN stainless steel and the geometry detail is shown in Fig. 4. Also for the TF model the magnetic permeability has been considered equal to the vacuum one  $\mu_{TF} = 4\pi \cdot 10^{-7}\text{ H/m}$ , while the electrical resistivity is that of the selected stainless steel evaluated at  $4.5\text{ K}$ :  $\rho_{el,TF} = 54.4 \cdot 10^{-8}\ \Omega\text{ m}$ .

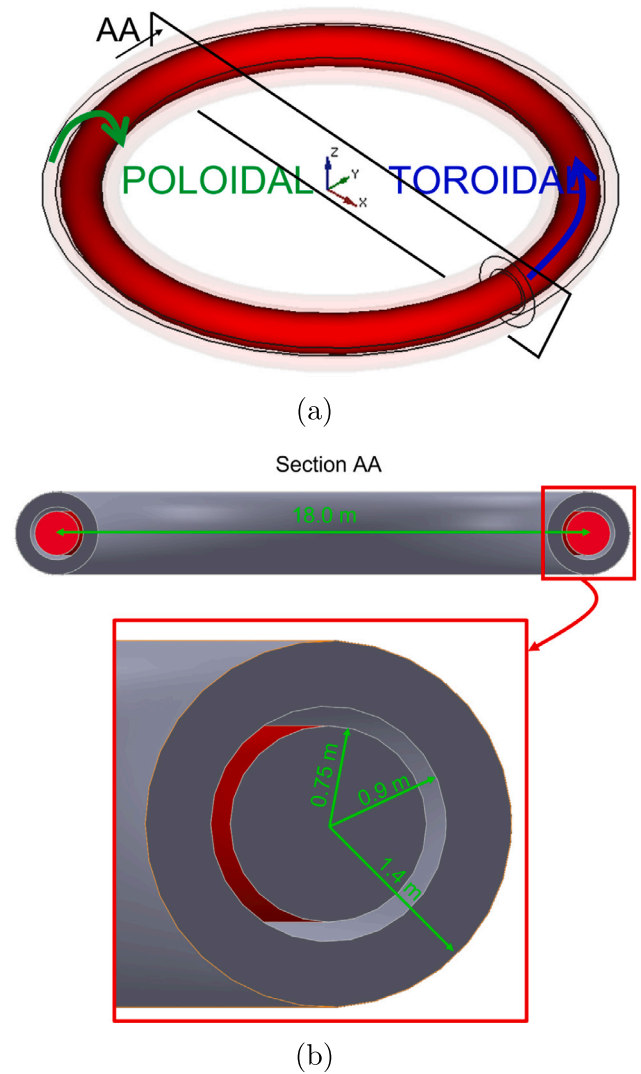


Fig. 1. Plasma current components as defined in the 3D-FOX model. In red the inner torus and in transparency the external torus (a). Their size is also shown (b).

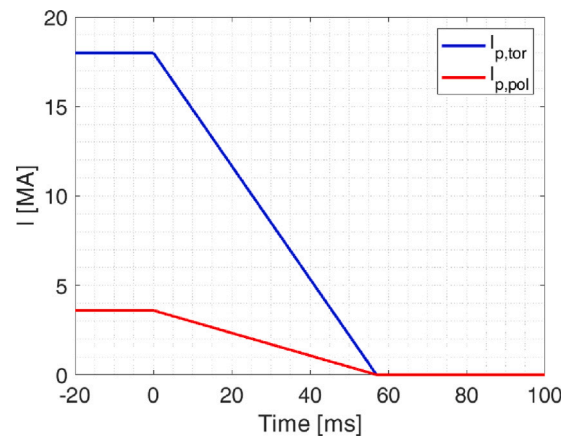


Fig. 2. Evolution of plasma current components during a MPD. The start of the disruption is set at  $t = 0\text{ ms}$ .

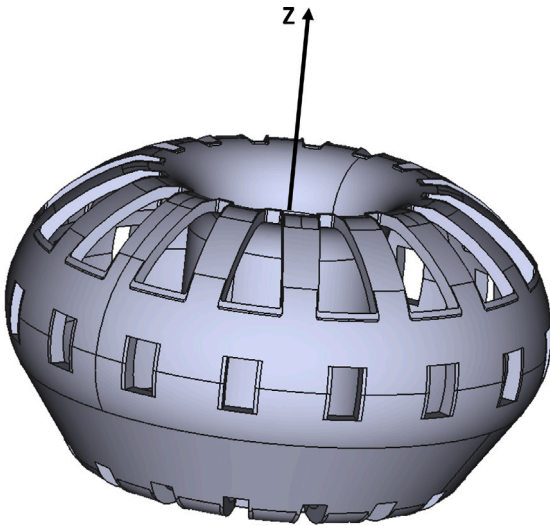


Fig. 3. VV CAD adopted as input for the FE model [14]. As a reference the z axis is shown too.

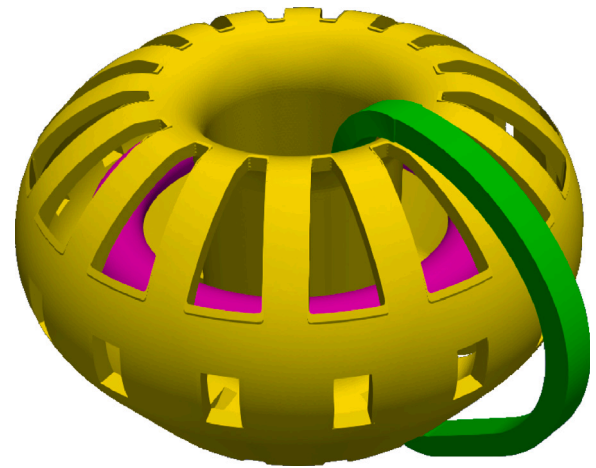


Fig. 5. Global view of the three main components of the model. In magenta the plasma, in yellow the VV and in green the TF coil.

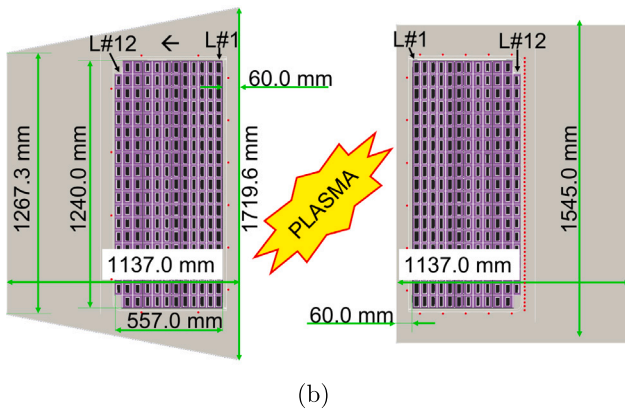
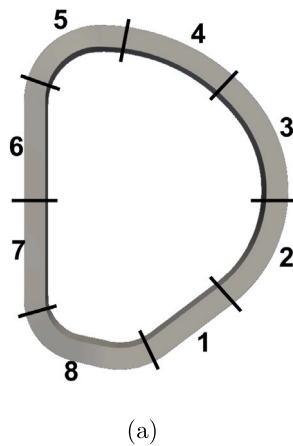


Fig. 4. TF coil casing side view on which the poloidal segmentation for power deposition averaging and 4C code structure model is shown (a), and the inboard (left) and outboard (right) equatorial cross sections of the TF coil with WP details (layer numbering and dimensions) are reported [15](b). The location of the Case Cooling Channels (CCCs) in the casing is highlighted with red spots as well.

2.4. Overall model and meshing

To perform the overall analysis the three models have been merged together and enclosed within a 30m radius sphere representing the external world, required to make the magnetic field line to close. In

Fig. 5 a global view of the three main component of the model (plasma, VV and TF coil) is shown. Only one of the 16 TF coils of the EU DEMO magnet system is included in the model since the contribution in the field distortion given by the presence of the neighboring coils is considered to be negligible on the scale of the simulation. Indeed, while the current induced within the VV is of the order of that of the plasma ( $\approx 10\text{MA}$ ), that induced in the casing of the TF coils is only  $\approx 10\text{kA}$ . Therefore, being the distance between two neighboring TF coils similar to (or even larger than) that between the coil and the VV, the magnetic field induced in a TF coil by the eddy currents in the casing of its neighbor is much smaller than that induced by the current in the VV. Moreover the time scale of the eddy current evolution within the TF coils casing is longer than that within the VV. Thus the time derivative of the magnetic field induced in the casing of a TF coil by the eddy currents in the casing of the neighboring magnet is much smaller than that due to the variation of the current in the VV. Both these considerations justify the assumptions of neglecting the effect of neighboring TF coils with respect to the contribution given by the VV. This choice allowed to reduce the computational cost of the simulation. The computational mesh has been produced using the open-source software gmsh [16] through a frontal Delaunay algorithm. The mesh has been built including appropriate local refinement in the region of interest in order to reduce as much as possible the computational cost eliminating useless cells (e.g. in the external air). The most refined region is the TF case one, to ensure accurate evaluation of the current induced there as well as the TF case power deposition, final aim of the work. In Fig. 6 a cross section of the computational domain shows the different mesh refinements. The choice of the different mesh refinement and of the dimension of the external sphere has been performed based on a grid independence analysis which allowed to guarantee the required accuracy of the results while keeping the computational cost reasonable. The problem has been solved with the A-formulation [9] and on the external surface of the computational domain, “far boundary” boundary conditions have been imposed, namely prescribing that  $\vec{A} \times \hat{n} = 0$ .

3. Electro-magnetic model results

The eddy currents induced within the VV and in the TF coil casing as well as the evaluation of the power deposited within the TF coil casing itself are discussed here.

The magnetic field variation responsible of the eddy current induction is represented here by means of the evolution of the plasma contribution to the magnetic field ( $\vec{B} - \vec{B}_0$ ,  $\vec{B}$  where is the total magnetic field and  $\vec{B}_0$  is the background constant magnetic field due to the magnet transport current) at WP center on the equatorial plane (Fig. 7).

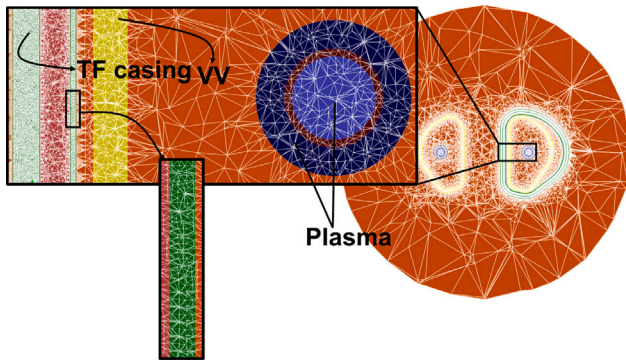


Fig. 6. Cross section of the computational domain to highlight the different mesh refinement.

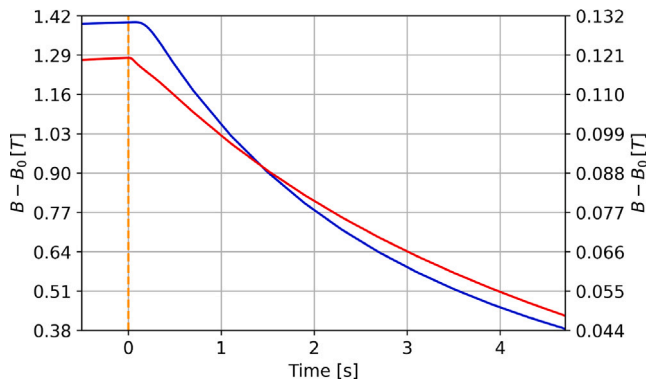


Fig. 7. Evolution of the plasma contribution to magnetic field at WP center on the equatorial plane at both inboard (blue, left axis) and outboard (red, right axis).

### 3.1. VV eddy currents

The driver of the problem is the decrease of the two components of the plasma current. According to Faraday’s law, in the conductive regions, currents are induced such that the field they are generating is opposing the variation of the driver field. This means that currents are expected in the VV in the same directions (toroidal and poloidal) of those of the plasma, with an orientation that should compensate the variation of the driver magnetic field. Due to the higher magnitude of the toroidal plasma current component, the toroidal component of the eddy current induced within the VV is expected to be the dominant. The expectation is reflected by the computed results. Indeed looking at the induced VV eddy current map on the equatorial plane evaluated at 600 ms (Fig. 8) from the MPD beginning it is possible to see that the current flow direction is the same as those of the plasma (reported in Fig. 1).

VV eddy current distribution at 600 ms is reported in Fig. 9 in a 3D view of the VV too, where it is possible to see how the current is mainly flowing where the material is continuous and so the electrical resistance reduced. Indeed, current density is strongly reduced in correspondence of the ports.

### 3.2. TF coil casing eddy currents

As discussed in the previous section, the major eddy current component is the toroidal one. Each TF coil in the EU DEMO magnet system is electrically insulated from the neighboring, preventing the possibility of having toroidal currents flowing from one TF to the others. For this reason the toroidal currents which are induced within the TF coil casing must flow in the cross section of the structure generating a loop all around the WP. In Fig. 10 is possible to observe the eddy

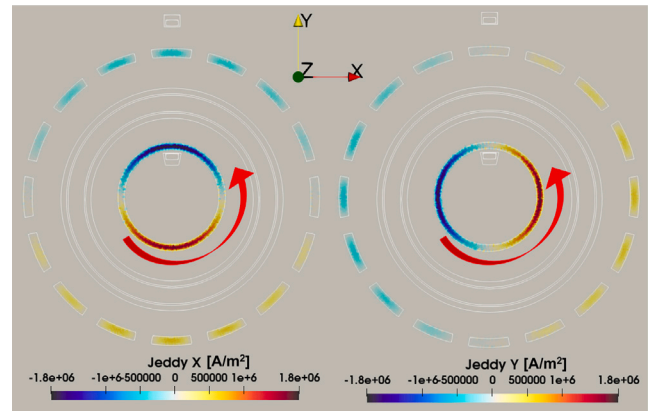


Fig. 8. VV eddy current toroidal components on the equatorial plane after 600 ms from the MPD beginning. The red arrows show the orientation of the current.

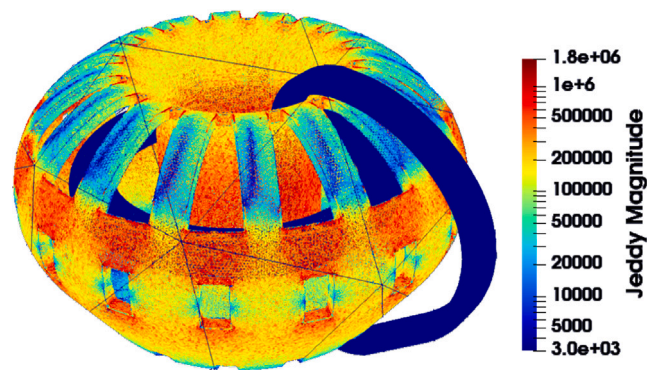


Fig. 9. 3D view of the eddy current module distribution within the VV after 600 ms from the MPD beginning.

current path within the TF coil casing right after the end of the MPD (60 ms). A zoom on a portion of the vertical inner leg highlights the above mentioned generation of toroidal current loop within the casing cross section. A major external loop can be observed “wrapping” the WP, but also a secondary loop can be seen in the nose region where sufficient conducting material is present to close the current loop. In the zoom it is also possible to appreciate the impact of the poloidal component of the current which is generating this sort of spiral path for the current. Moreover, it is possible to observe that non-negligible differences arise between the upper and lower part of the TF coil casing, with higher current density in the top part. This difference is given by the non symmetric shape of the TF coil with respect to the equatorial plane. Indeed, the bottom part is farther from the plasma (which is centered at  $z = 0$  and is driving the transient in these parts of the TF coil casing) than the upper one. This dependency has been confirmed moving down the plasma center (not shown here) and observing a more even distribution of the current density within the TF coil casing.

Moving on in the transient, the current distribution within the TF coil casing is evolving, showing macroscopic differences. Looking at the same zoom on the vertical leg presented in Fig. 10 after 600 ms of transient, it is possible to observe how the rotation direction of the induced current loop has been reversed with respect to the end of the plasma disruption (Fig. 11).

The reason for this change of rotation direction is given by the evolution of the derivative of the major driver current, which for the TF inner leg is the VV eddy current. Indeed, during the plasma disruption the current induced within the VV is increasing, while, later on, the VV eddy current peak is reached and it start decreasing. As a consequence the TF coil casing eddy currents are changing rotation direction as well

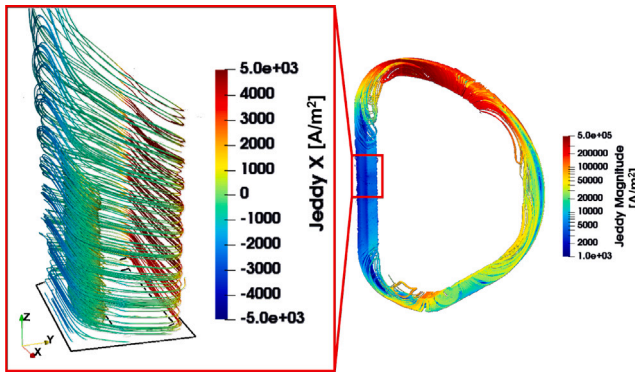


Fig. 10. Eddy current distribution induced within the TF coil casing right after the end of MPD (60 ms after the MPD beginning).

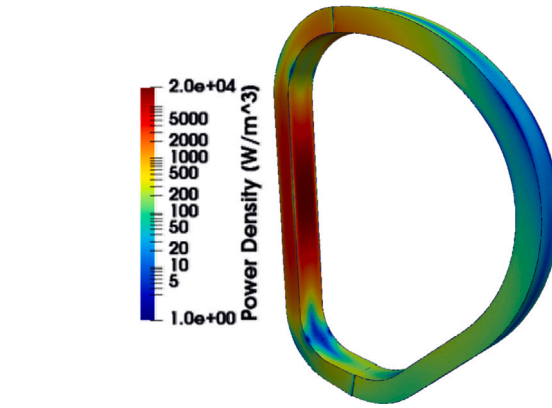


Fig. 12. Eddy current power deposition within the TF coil casing after 600 ms from MPD beginning.

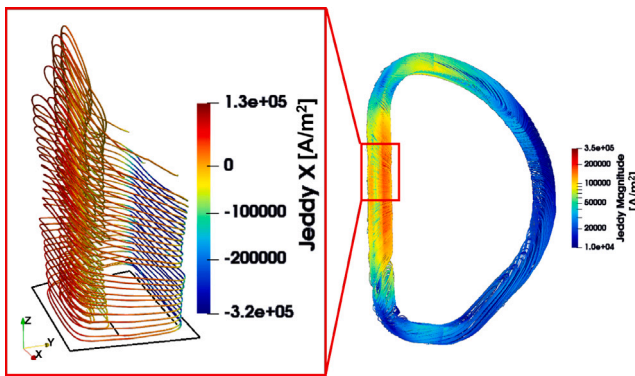


Fig. 11. Eddy current distribution induced within the TF coil casing after 600 ms from MPD beginning.

as the derivative of VV eddy currents. Moreover, comparing the eddy current distribution shown in Figs. 10 and 11, it is possible to realize that the point at maximum current density is moving along the D-shape of the coil. This will have an influence on the evolution of the local power deposition, to be considered in the TH simulation.

### 3.3. TF coil casing power deposition

Given the electrical resistivity of the TF coil structure, the eddy currents induced in it are depositing power by Joule effect according to Ohm's law. The distribution of the power deposited is strictly related to the distribution of eddy currents induced within the casing, as it is possible to observe from Fig. 12 where the power distribution is recalling that of the currents reported in Fig. 11. Knowing the power deposition distribution is possible to integrate it all over the domain, computing the overall Joule heat deposited within the TF coil casing during the transient. This power deposition translates into an overall energy deposition for each coil casing of almost 0.5 MJ. This value is of the same order of magnitude of those computed in [7]. Direct quantitative comparison is impossible to be performed due to the difference in size between the two considered geometries and to the different plasma current evolution considered in the analysis. The evolution of the total power is shown in Fig. 13.

The total power evolution shows an initial peak in correspondence of the MPD event, followed by a part of the transient in which the power decrease is slower due to the different time scales of the local power deposition evolution in different casing points. Indeed, as shown in Figs. 10 and 11, the maximum power density is moving along the TF D-shape. The different time scales of the power deposition can be better appreciated looking at the average power density computed within the

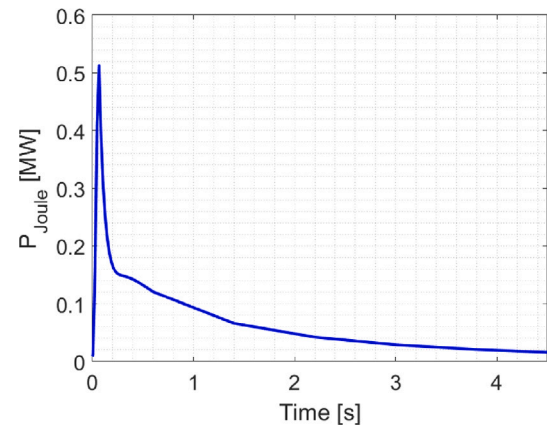


Fig. 13. Total power deposition evolution in the entire TF coil casing.

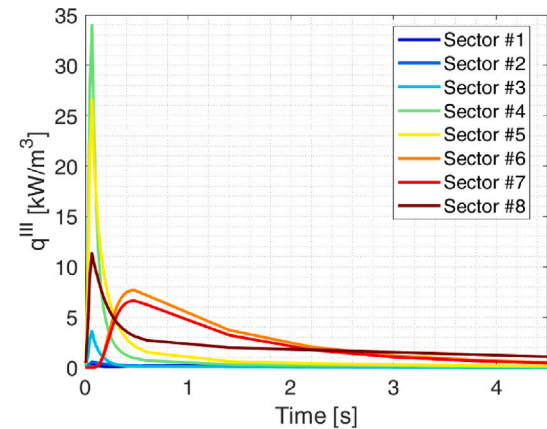


Fig. 14. Average power density in each of the 8 TF coil casing sectors considered in this analysis and adopted as input to the TH simulation.

eight segments (reported in Fig. 4(a)) of the TF coil casing adopted for the structure module of the 4C code (Fig. 14). Indeed, the segments of the vertical leg (6 and 7) show a qualitative evolution different with respect to the others, characterized by a delayed peak, which causes the slow down of the integral power decrease observed in Fig. 13. The power evolution within the vertical leg is showing this delayed peak since it is mainly driven by the VV eddy currents and is not influenced by the plasma, whose effect is very effectively shielded by the innermost part of the VV.

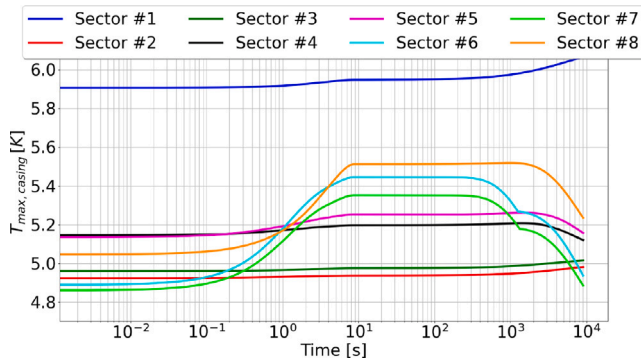


Fig. 15. Maximum temperature evolution in each casing sector of the TF coil.

#### 4. TH effects of the MPD on the TF coil

The power deposited within the TF coil casing must be carefully considered in the TH analysis, since it can lead to an erosion of the SC temperature margin. For this reason the 4C code model of the EU DEMO WP, developed in [17] and adapted to the selected WP configuration (concept 1 in [18]), has been adopted for the TH simulation of the MPD. Due to the lack of information on the other thermal loads on the WP (e.g. AC losses), the TH model has been adopted here mainly for the evaluation of the temperature increase of the casing and the power transfer from casing to WP. However, the TH model is ready to perform the complete analysis once all the heat loads will be available and give as inputs. The computed averaged power within the 8 segments presented in Fig. 4(a) is used as input to the 4C code as already done in [9].

##### 4.1. TH simulation setup

As mentioned above, the driver is the power deposition due to eddy currents. Two additional thermal loads on the structures are considered in this analysis, which are the conductive load coming from the gravity support and the radiative heat load on magnet lateral surfaces. The first is assumed to be equal to 7 W [19] and localized in sector 1, the second to 0.12 W/m<sup>2</sup> on the casing surfaces exposed to the thermal shield [20]. From the TH point of view, the boundary conditions (BCs) have been imposed by a simplified circuit model [17] which, thanks to mass and energy balances, from the computed mass flows at WP and CCCs inlet and outlet evaluates the inlet and outlet pressure values and imposes the inlet temperature, both for WP and for the Casing Cooling Channels (CCCs), to 4.5 K. In this work it has been assumed that the cryoplant is removing the transient heat load at the same time scale of its extraction from the magnet by the He flow. This is not representative of the real machine operation, which will include heat load smoothing techniques, but these solutions have not been assessed yet for DEMO. As a consequence these results may be used as a starting point for the development of the above mentioned solutions, based e.g. on those already proposed for ITER [21].

##### 4.2. TH simulation results

The power deposited within the TF coil casing is increasing its temperature and is partly removed by the CCCs and partly directed to the WP, from which it is removed by the He cooling the conductors. The casing temperature increase is monitored by means of the maximum casing temperature in each segment and is reported in Fig. 15. From this figure it is possible to observe that the largest temperature increase is detected in sectors 6, 7 and 8, where there is the largest energy deposited (despite the peak power is lower than in sectors 4 and 5 the peak is larger and so the deposited energy). The temperature in sector 1

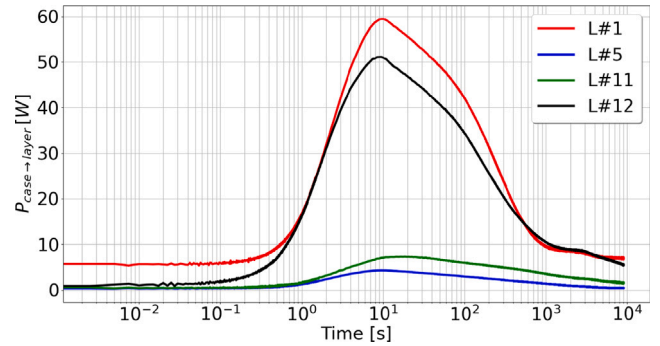


Fig. 16. Power directed from TF coil casing towards the WP in each layer.

increases monotonically because there the (constant) conductive heat load from the gravity support is deposited. This energy contribution is predominant with respect to that provided by the induced eddy currents. The same trend can be observed in sectors 2 and 3 as well, which are directly in contact with sector 1 and for which the heat load given by eddy current is low.

The power transferred to the WP from the solids is reported in Fig. 16. It shows that the most heated layers are the first and the last, which are in contact for their entire length with the coil casing.

This energy transfer to the WP is responsible for the SC temperature margin erosion, together with the AC losses and WP eddy currents (that can be computed by different models such as [22] or [3]) and other thermal loads (e.g. nuclear heat load).

#### 5. Conclusions and perspective

In this work the VV, TF and plasma models have been developed in the 3D-FOX tool, such that it was possible to apply it to the computation of eddy currents induced both in the VV and in the TF coil casing during a MPD. The model of the VV, not included in previous 3D-FOX versions, is fundamental for the simulation of such kind of transient since the currents induced on it strongly influence the evolution of the magnetic field in correspondence of the TF coil casing, thus affecting the currents induced there. The simulation results show that the current density is not evenly distributed along the TF coil casing and is influenced by the plasma proximity and by the shielding effect provided by the VV (mainly in the inner leg) Due to this shielding effect a delayed peak in local power deposition in the inner leg is detected with respect to the remaining part of the casing. The computed power deposition has been used as input to the TH simulation of MPD effect in the TF coil. From the TH analysis the casing temperature increase and the power transferred to the WP have been computed. This power contributes to the erosion of the SC temperature margin. However, besides heat load due to the eddy current in the casing, other contributions should be considered in future works to better assess the temperature margin (e.g., AC losses, WP eddy currents and nuclear heat load in the WP). Moreover, the final results are certainly subject to uncertainties due to the preliminary stage of the design of the various components of the EU DEMO reactor, but the developed model will be capable to deal with any input update as soon as they will be available.

In perspective, the fast discharge as a consequence of the MPD is foreseen to evaluate the impact of the overall transient foreseen in case of an MPD. Parametric analysis on the delay time to trigger the discharge after the MPD event can be performed to find out the optimal shut down solution.

The introduction of periodic boundary conditions in the model for the sake of reducing the computational cost has not been implemented here for the current limitations in the software: it is foreseen in future works.

## Declaration of competing interest

The authors declare that they have no known competing financial interests or personal relationships that could have appeared to influence the work reported in this paper.

## Data availability

No data was used for the research described in the article.

## Acknowledgments

This work has been carried out within the framework of the EUROfusion Consortium, funded by the European Union via the Euratom Research and Training Programme (Grant Agreement No 101052200 — EUROfusion). Views and opinions expressed are however those of the authors only and do not necessarily reflect those of the European Union or the European Commission. Neither the European Union nor the European Commission can be held responsible for them.

## References

- [1] Francesco Romanelli, P. Barabaschi, D. Borba, G. Federici, L. Horton, R. Neu, D. Stork, H. Zohm, Fusion Electricity: A Roadmap to the Realization of Fusion Energy, Efd, 2012.
- [2] R. Bonifetto, M. De Bastiani, A. Di Zenobio, L. Muzzi, S. Turtù, R. Zanino, A. Zappatore, Analysis of the thermal-hydraulic effects of a plasma disruption on the DTT TF magnets, *IEEE Trans. Appl. Supercond.* 32 (6) (2022) 1–7.
- [3] Lorenzo Bortot, Bernhard Auchmann, Idoia Cortes Garcia, Herbert De Gerssem, Michal Maciejewski, Matthias Mentink, Sebastian Schöps, Jeroen Van Nugteren, Arjan P. Verweij, A coupled A–H formulation for magneto-thermal transients in high-temperature superconducting magnets, *IEEE Trans. Appl. Supercond.* 30 (5) (2020) 1–11.
- [4] Lorenzo Cavallucci, Marco Breschi, Pier Luigi Ribani, Andrew V. Gavrilin, Hubertus W. Weijers, Patrick D. Noyes, A numerical study of quench in the NHMFL 32 T magnet, *IEEE Trans. Appl. Supercond.* 29 (5) (2019) 1–5.
- [5] M. Sugihara, M. Shimada, H. Fujieda, Yu Gribov, K. Ioki, Y. Kawano, R. Khayrutdinov, V. Lukash, J. Ohmori, Disruption scenarios, their mitigation and operation window in ITER, *Nucl. Fusion* 47 (4) (2007) 337.
- [6] Duck-Hoi Kim, Dong-Keun Oh, Sunil Pak, Hogun Jhang, Jaeyoul Lee, Vladimir Rozov, Eddy current induced electromagnetic loads on shield blankets during plasma disruptions in ITER: A benchmark exercise, *Fusion Eng. Des.* 85 (10–12) (2010) 1747–1758.
- [7] F. Cau, D. Bessette, G. D'Amico, A. Portone, G. Rubinacci, P. Testoni, Salvatore Ventre, Fabio Villone, Joule losses in the ITER cold structures during plasma transients, *IEEE Trans. Appl. Supercond.* 26 (4) (2016) 1–5.
- [8] Raffaele Albanese, Guglielmo Rubinacci, Integral formulation for 3D eddy-current computation using edge elements, *IEE Proceedings A (Physical Science, Measurement and Instrumentation, Management and Education, Reviews)* 135 (7) (1988) 457–462.
- [9] Roberto Bonifetto, Marco De Bastiani, Roberto Zanino, Andrea Zappatore, 3D-FOX—A 3D transient electromagnetic code for eddy currents computation in superconducting magnet structures: DTT TF fast current discharge analysis, *IEEE Access* 10 (2022) 129552–129563.
- [10] F. Hecht, New development in FreeFem++, *J. Numer. Math.* 20 (3–4) (2012) 251–265.
- [11] L. Savoldi Richard, F. Casella, B. Fiori, R. Zanino, The 4C code for the cryogenic circuit conductor and coil modeling in ITER, *Cryogenics* 50 (3) (2010) 167–176.
- [12] Giuseppe Ramogida, EM Model for DEMO 2017 Baseline and Perturbation Simulations, Technical Report, EUROfusion, 2018, Available online: <https://idm.euro-fusion.org/default.aspx?uid=2MWEM8M>.
- [13] R. Lombroni, F. Giorgetti, G. Calabrò, P. Fanelli, G. Ramogida, Using MAXFEA code in combination with ANSYS APDL for the simulation of plasma disruption events on EU DEMO, *Fusion Eng. Des.* 170 (2021) 112697.
- [14] Curt Gliss, June-2017 DEMO Reference Configuration model, Technical Report, EUROfusion, 2017, Available online: <https://idm.euro-fusion.org/default.aspx?uid=2MUNPL>.
- [15] V. Corato, P. Bruzzone, N. Bykovskiy, G. Celentano, A. della Corte, F. Demattè, S. Fink, W.H. Fietz, L. Muzzi, X. Sarasola, K. Sedlak, A. Torre, L. Zani, G. Federici, Strategy for developing the EU-DEMO magnet system in the concept design phase, *IEEE Trans. Appl. Supercond.* 32 (6) (2022) 1–7.
- [16] Christophe Geuzaine, Jean-François Remacle, Gmsh: A 3-D finite element mesh generator with built-in pre-and post-processing facilities, *Internat. J. Numer. Methods Engrg.* 79 (11) (2009) 1309–1331.
- [17] Roberto Zanino, Roberto Bonifetto, Ortensia Dicuonzo, Luigi Muzzi, Giuseppe F. Nallo, Laura Savoldi, Simonetta Turtù, Development of a thermal-hydraulic model for the European DEMO TF coil, *IEEE Trans. Appl. Supercond.* 26 (3) (2016) 1–6.
- [18] V. Corato, C. Vorpahl, K. Sedlak, V.A. Anvar, J. Bennet, M.E. Biancolini, F. Bonne, R. Bonifetto, D.P. Boso, A. Brighenti, P. Bruzzone, G. Celentano, A. della Corte, G. De Marzi, V. D'Auria, F. Demattè, A. Dembkowska, O. Dicuonzo, C. Fiamozzi Zignani, W.H. Fietz, C. Frittitta, L. Giannini, F. Giorgetti, R. Guarino, R. Heller, C. Hoa, M. Huguet, G. Jiolat, M. Kumar, B. Lacroix, M. Lewandowska, N. Misiara, L. Morici, L. Muzzi, D.S. Nickel, S. Nicollet, A. Nijhuis, F. Nunio, C. Portafaix, X. Sarasola, L. Savoldi, I. Tiseanu, G. Tomassetti, A. Torre, S. Turtù, D. Uglietti, R. Vallcorba, K.-P. Weiss, R. Wesche, M.J. Wolf, K. Yagotintsev, L. Zani, R. Zanino, A. Zappatore, The DEMO magnet system – status and future challenges, *Fusion Eng. Des.* 174 (2022) 112971.
- [19] Sofia Viarengo, Andrea Allio, Daniela P Boso, Laura Savoldi, Kamil Sedlak, Valentina Corato, Analysis of the effects of thermal anchors on the reduction of the parasitic load to the EU-DEMO TF coils, *Fusion Eng. Des.* 169 (2021) 112485.
- [20] Matti Coleman, Definition of the External Static Radiative and Conductive Heat Loads on the TF Coil Casing, Technical Report, EUROfusion, 2016, Available online: <https://idm.euro-fusion.org/default.aspx?uid=2N6VWA>.
- [21] A. Alekseev, D. Arslanova, V. Belyakov, D. Bessette, I. Gornikel, V. Kalinin, M. Kaparkova, N. Mitchell, L. Serio, N. Shatil, S. Sytchevsky, V. Vasiliev, Control strategy for mitigation of pulsed heat load transferred to ITER cryoplant from magnets, *Fusion Eng. Des.* 121 (2017) 1–6.
- [22] P. Bauer, M. Breschi, L. Cavallucci, J.L. Duchateau, F. Gauthier, A. Torre, B. Turck, Description of the AC loss model for the ITER central solenoid during a plasma scenario, *IEEE Trans. Appl. Supercond.* 32 (6) (2022) 1–5.